Applied Catalysis B: Environmental 140–141 (2013) 363–377

Contents lists available at SciVerse ScienceDirect

Applied Catalysis B: Environmental

journal homepage: www.elsevier.com/locate/apcatb

Improved activity and stability in CO oxidation of bimetallic Au–Cu/TiO_2 catalysts prepared by deposition–precipitation with urea

Alberto Sandoval[a], Catherine Louis[b], Rodolfo Zanella[a,*]

[a] Centro de Ciencias Aplicadas y Desarrollo Tecnológico, Universidad Nacional Autónoma de México, Circuito Exterior S/N, Ciudad Universitaria, A. P. 70-186, Delegación Coyoacán, C.P. 04510 México D.F., Mexico

[b] Laboratoire de Réactivité de Surface, UMR CNRS 7197, Université Pierre et Marie Curie-UPMC, 4, place Jussieu, 75252 Paris Cedex 05, France

ARTICLE INFO

Article history:
Received 11 February 2013
Received in revised form 14 April 2013
Accepted 16 April 2013
Available online 24 April 2013

Keywords:
CO oxidation
Gold
Copper
Bimetallic catalysts

ABSTRACT

Au–Cu bimetallic catalysts supported on TiO_2 were prepared for the first time by sequential deposition–precipitation with the urea method, copper first then gold. Au–Cu catalysts with four different Au:Cu atomic ratios were synthesized (1:0.4 to 1:1.2). This method allowed quantitative deposition of both copper and gold and the formation of small metal particles. Characterization by TPR and by DRIFTS coupled with CO adsorption showed that when the samples were activated in air at 300 °C gold was present in metallic form, copper in the form of an oxide, and Au and Cu were in interaction, probably forming a Au/CuO/TiO_2 system. When the catalysts were activated in hydrogen at 300 °C, the metal particles were smaller (2 nm) and bimetallic. The activation of Au–Cu catalysts in air at 300 °C produced more active catalysts than the activation under hydrogen at the same temperature. However, whatever the activation procedure, the highest catalytic activity in CO oxidation was obtained for the catalyst with an Au:Cu ratio of 1:0.9. This calcined catalyst also presented a TOF almost 3 times higher and a better temporal stability than monometallic gold catalysts in the reaction of CO oxidation at 20 °C. Compared to monometallic catalysts, the better catalytic results obtained with calcined Au–Cu/TiO_2 indicate a promoting effect between gold and copper oxide in the reaction of CO oxidation.

1. Introduction

Frequently, the physical and chemical properties of bimetallic particles are found to be very different from their single metal counterparts. In particular, various physical properties and electronic structures are found to significantly vary as a function of composition and particle size. Catalytic activity and selectivity of bimetallic systems can be found to be superior to either of the corresponding monometallic catalysts [1–3]. The enhanced properties of bimetallic catalysts are generally attributed to either ensemble or ligand effects although other factors related to particle size effects, support effects, and catalyst stability have been invoked [4].

Now, it is well established that gold nanoparticles supported on oxide supports are active in many reactions of both industrial and environmental importance [5]. The most remarkable catalytic properties of supported gold have been obtained for the reaction of CO oxidation at ambient temperature [5–8]. Although supported gold nanoparticles have proven to be extremely active, most Au catalysts still suffer from rapid deactivation, which is a drawback for practical applications. The deactivation mechanism is often attributed to the agglomeration/sintering of Au particles [9–12], the formation of carbonates adsorbed on the active sites [13,14], the consumption of catalyst surface OH groups during CO oxidation, or the change of oxidation state of gold [15,16].

In addition, both experimental works and theoretical calculations have shown that the adsorption and activation of O_2 are important steps in the CO oxidation reaction [17–20]. Whereas gold nanoparticles are known to adsorb CO molecules on their low coordination sites, they do not strongly adsorb and activate oxygen molecules [21,22]. Thus, the oxide support is supposed to play an important role in the activation of oxygen, especially those with good redox property. A way to improve the Au capability to activate oxygen could be to combine gold within bimetallic particles with a second metal able to dissociate O_2. Activated O_2 could easily react with adsorbed CO on a neighboring gold atom and produce CO_2.

It has been proposed than in Au–Cu systems, Cu can facilitate the activation of molecular oxygen [23], and that bimetallic Au–Cu alloy catalysts are significantly more active than monometallic Cu and Au catalysts in the CO oxidation reaction because of a synergistic interaction between Cu and Au [2,24–27]. It has also been shown that Au–Cu catalysts are also more stable under reaction conditions in the oxidation of CO and more resistant against sintering induced by high-temperature calcination [25,27,28].

* Corresponding author. Tel.: +52 55 56228635; fax: +52 55 55500654.
E-mail address: rodolfo.zanella@ccadet.unam.mx (R. Zanella).

0926-3373/$ – see front matter © 2013 Elsevier B.V. All rights reserved.
http://dx.doi.org/10.1016/j.apcatb.2013.04.039

Recently, Liu et al. [29] showed that whereas gold remained as Au^0 under any treatment conditions, copper was very sensitive to the treatment temperature and atmosphere in Au–Cu/SBA15 catalysts prepared by a two-step adsorption method. They proposed that the initially formed Au_3Cu_1 intermetallic phase in reduced catalysts transformed into gold core particles decorated with tiny CuO_x patches during CO oxidation and that CO adsorbed on Au^0 reacted with activated oxygen provided by the neighboring CuO_x, thus enhancing greatly the activity for CO oxidation. A similar phenomenon was observed by Bauer et al. [27] when alloyed Au–Cu supported on SiO_2 was calcined at 400 or 500 °C; they observed the oxidation of Cu^0 and proposed the transformation of Au–Cu alloy particles into a Au–CuO_x composite. They also found that whereas the Au–Cu/SiO_2 alloy catalysts were inactive for CO oxidation, the catalytic activity dramatically increased after calcination. According to several papers [23,27,29] the most active phase in CO oxidation is not a Au–Cu alloy but a Au–CuO combination.

A few methods have been used to prepare supported Au–Cu catalysts. The impregnation method generated particles larger than 10–15 nm on TiO_2 [30] and CeO_2 [31–33]. The deposition–precipitation method at fixed pH by addition of ammonia or co-precipitation has also been used to prepare Au–Cu catalysts supported on TiO_2 [24,34–36], Al_2O_3 [28], and SBA-15 [23] yielded average particle sizes between 2 and 5 nm. Cu impregnation together with Au deposition–precipitation have also been used to obtain Au–Cu/TiO_2 catalysts [24,34]; the average particle size reported in reference [24] was 2–3 nm, whereas in reference [34] it was not reported. Preformed Au–Cu colloidal nanoparticles have also been adsorbed [37] or impregnated [38] on TiO_2, the average particle sizes varied from 2 to 8 nm, the disadvantage of this method is that when preformed nanoparticles are used to impregnate a support, they are always larger than the colloidal nanoparticles (of about 2 nm) after thermal treatment performed to remove the stabilizing agents. Other methods involving successive adsorption of gold ($HAuCl_4$) or ($Au(en)_2Cl_3$) then copper ($Cu(NO_3)_2$ or $Cu(C_2H_3O_2)_2$) have been used to prepare Au–Cu supported on SiO_2 [26,27] or SBA 15 [25,29] producing average particle sizes of 3–4 nm. In some cases, gold is chemically reduced before adsorption of Cu species [25,26,29,39].

The goal of this work was to explore the possibility of preparing Au–Cu catalysts supported on a reducible TiO_2 support by a method different from those already cited, *i.e.*, by the deposition–precipitation with urea method, which has been proved to be a very efficient method to prepare Au/TiO_2 catalysts [40,41]; then to study the activity and stability of these catalysts in CO oxidation as a function of the conditions of activation (gas and temperature), and try to elucidate the nature of the interaction between gold and copper atoms and the surface composition of the catalysts to explain their catalytic behavior. To avoid uncontrolled precipitation of copper in the presence of the gold precursor ($HAuCl_4$), sequential deposition–precipitation of copper first then of gold was preferred to co-deposition–precipitation.

2. Experimental

2.1. Catalyst preparation

2.1.1. Preparation of monometallic samples

Titania Degussa P25 was used as support (45 $m^2\,g^{-1}$, nonporous, 70% anatase and 30% rutile, purity >99.5%). Commercial $HAuCl_4{\cdot}3H_2O$ and $Cu(NO_3)_2{\cdot}2.5H_2O$, both from Aldrich, were used as gold and copper precursors. Before preparation, TiO_2 was dried in air at 100 °C for at least 24 h to desorb species adsorbed on the surface. The nominal metal loadings in the monometallic catalysts were 4 wt.% for Au and 1.4 wt.% for Cu, equivalent to 0.56 at.% for both samples.

The preparation of the 4 wt.% Au/TiO_2 sample was performed by deposition–precipitation with urea (DPU) in the absence of light, following the previously reported procedure [40–42]. Briefly, the gold precursor, $HAuCl_4$ (4.2×10^{-3} M), and urea (0.42 M) were dissolved in 50 mL of distilled water; the initial pH of the solution was 2.4 Then, 1 g of titania was added to this solution. Thereafter, the suspension temperature was increased to 80 °C and kept constant for 16 h under stirring. Urea decomposition led to a gradual rise in pH to 7.2.

The preparation of the 1.4 wt.% Cu/TiO_2 sample was performed according to the same method with 1 g of TiO_2 and 54 mL of an aqueous solution containing $Cu(NO_3)_2$ (4.2×10^{-3} M) and urea (0.42 M). The initial pH was ~3.2. The suspension was vigorously stirred for 4 h at 80 °C. The final pH was 7.4.

After the deposition–precipitation procedure, all samples were centrifuged, washed with water and centrifuged four times, and dried under vacuum for 2 h at 80 °C. After drying, the samples were stored at room temperature in a desiccator under vacuum, away from light in order to prevent any alteration [42].

2.1.2. Preparation of bimetallic samples

For these samples, the gold nominal loading was 4 wt.%, whereas that for copper was chosen to synthesize Au–Cu catalysts with different Au:Cu atomic ratios: 1:0.5, 1:0.75, 1:1 and 1:1.5. A sequential deposition method was used to prepare these catalysts. Copper was first deposited on TiO_2 according to the DPU method described above. After being dried at 80 °C for 2 h, gold was also deposited by DPU as previously described. Then, these samples were washed, dried, and stored, also as described above. The samples were identified as Au–Cu followed by the nominal Au/Cu atomic ratio, *e.g.*, Au–Cu 1:0.5.

2.2. Catalytic activity

The CO oxidation reaction was studied in a flow reactor at atmospheric pressure and increasing temperature from −5 to 500 °C (light off test). 40 mg of dried catalyst was first activated *in situ* in a flow of 40 mL min^{-1} of hydrogen or air with a heating rate of 2 °C min^{-1} up to the final chosen temperature, between 150 and 500 °C, followed by a temperature plateau of 2 h. After this treatment, the sample was cooled to −5 °C under the same gas. The reactant gas mixture (1 vol.% CO and 1 vol.% O_2 balanced with N_2) was introduced with a total flow rate of 100 mL min^{-1}, and a heating rate of 2 °C min^{-1}. The gases were analyzed with an Agilent Technologies 6890N online gas chromatograph equipped with a FID detector, a methanizer and a HP Plot Q column. To measure the reaction rates and the activation energies, experimental conditions were determined so as to perform these measurements in kinetic regime. For that purpose, different dilutions of Au–Cu samples in titania (the same one as the support) were prepared (*e.g.*, 60% dilution: 60% sample + 40% titania) using catalysts sieved between 100 and 250 μm then calcined *in situ* at 300 °C. The [reaction rate at 50 °C]/[concentration of active material] ratio was found to be almost constant (Koros–Nowak test) for dilutions between 40 and 60% of active material; for a higher concentration of sample of 65% the [reaction rate]/[concentration] ratio increased considerably. As a consequence, the reaction rates and Arrhenius plots were determined with catalysts with a dilution of 60%. The turnover frequencies (TOF), number of molecules of CO converted per surface atom of gold particles and per second, were determined from the reaction rates obtained in the kinetic regime and the dispersion of gold (surface atoms/total atoms in the particle). The dispersion of gold was calculated with the assumption that gold particles were

Table 1
Theoretical and actual Au and Cu loadings in the studied catalysts.

Nominal composition	Metal loading, wt.%				Actual Au/Cu atomic ratio
	Nominal Au loading	Actual Au loading	Nominal Cu loading	Actual Cu loading	
Au	4	3.8	0	0	–
Cu	0	0	1.38	1.20	–
Au–Cu 1:0.5	4	3.8	0.68	0.55	Au–Cu 1:0.4
Au–Cu 1:0.75	4	3.8	1.04	0.84	Au–Cu 1:0.7
Au–Cu 1:1	4	3.8	1.38	1.15	Au–Cu 1:0.9
Au–Cu 1:1.5	4	4	2.1	1.73	Au–Cu 1:1.2

cuboctahedral with a hexagonal face in contact with the titania surface.

Stability of the catalysts *vs.* time on stream was examined at 20 °C during a 24-h run, using 40 mg of catalyst activated *in situ* in air at the same heating rate and temperature plateau as described above.

2.3. Characterization techniques

The chemical analysis of Au and Cu in the dried samples was performed by ICP in a Perkin Elmer Optima 4300 DV optical emission spectrometer. The Au and Cu weight loadings were expressed in grams of each metal per gram of sample.

Diffuse reflectance UV–vis spectra of the catalysts were obtained using a CARY 5000 (UV-VIS-NIR) spectrophotometer equipped with a Praying Mantis and a high temperature reaction chamber (Harrick). The spectra were recorded during the activation thermal treatment. In each experiment, approximately 25 mg of the dried sample were packed in the sample holder and pretreated *in situ* under hydrogen or air flow (30 mL min^{-1} and 2 °C min^{-1}) up to the chosen temperature, followed by a 30-min-plateau. A spectrum of Teflon (from Aldrich) was used as reference.

The hydrogen temperature programmed reduction (H_2-TPR) study of the dried catalysts was performed in a RIG-150 unit under a flow of 10% H_2/Ar gas mixture (30 mL min^{-1}) and with a heating rate of 10 °C min^{-1} from room temperature to 400 °C. H_2O produced during the reduction process was trapped before the TCD detector.

After *ex situ* thermal treatment under the same conditions as for the CO oxidation reaction, the samples were examined by transmission electron microscopy in a Jeol-2010 FasTem analytical microscope equipped with a Z-contrast annular detector and an EDS detector. The average size of gold particles and the histograms of particle sizes were established from the measurement of 800 to 1000 particles. The size limit for the detection of the metal particles on TiO_2 was about 0.6 nm. The average particle diameter d_s was calculated using the following formula: $d_s = \sum n_i d_i / \sum n_i$, where n_i is the number of particles of diameter d_i. The standard deviation was calculated with the formula: $\sigma = [\sum (d_i - d_s)^2 / \sum n_i]^{1/2}$. Micro-EDS measurements were performed over about 40 individual particles, randomly selected in different zones of the catalyst. The Cu and Au atomic values obtained are qualitative because no calibration of the EDS-detector was performed with an Au–Cu alloy standard.

CO adsorption was followed by FTIR spectroscopy to characterize the metallic surface. The experiments were carried out in a Nicolet 670FT-IR spectrophotometer equipped with a Praying Mantis for DRIFT spectroscopy and a low/high temperature reaction chamber by Harrick. In each experiment, approximately 25 mg of dried sample were packed in the sample holder and pretreated *in situ* under hydrogen or air flow (30 mL min^{-1}, heating rate 2 °C min^{-1}) up to the chosen temperature followed by a plateau for 1 h. After the thermal treatment, the sample was cooled to room temperature under the same gas flow and then purged with N_2 before the introduction of 5% CO in N_2 (30 mL min^{-1}). A spectrum recorded under N_2 was used as reference, then several spectra were recorded under the CO flow until the band intensity was stable; afterwards, temperature was increased under CO, and the spectra were recorded at increasing temperatures.

3. Results

3.1. Elemental analysis

Let us remember that the nominal metal loadings of the monometallic catalysts were chosen to be equal to 4 wt.% Au, for Au/TiO_2, and 1.4 wt.% Cu, for Cu/TiO_2, which corresponds to 0.56 at.% for both samples. Table 1 compares the nominal and the measured gold and copper loadings in wt.% and the Au:Cu atomic ratios for the Au–Cu samples. As expected from former studies on gold catalysts [40,41,43], the actual gold loadings are very close to the theoretical value (4 wt.%), whether the catalyst is mono or bimetallic. In the case of copper, it is between 81 and 83% of the nominal loading, whether the catalyst is mono or bimetallic, confirming that Cu can be deposited by this method [44] and that Cu is not leached during Au deposition. In the following, the Au–Cu samples are designated by their actual loadings.

3.2. CO oxidation

Fig. 1a shows the conversion of CO as a function of the reaction temperature for the four Au–Cu/TiO_2 catalysts activated under air at 300 °C. The results obtained for the monometallic catalysts are also reported for comparison. The Au/TiO_2 sample is already active at 0 °C (CO conversion ≈62%) whereas Cu/TiO_2 is completely inactive below 75 °C. It is interesting to note that in the range of temperatures at which Cu/TiO_2 is completely inactive (<75 °C), the Au–Cu samples are more active than gold except for Au:Cu 1:0.4, which is not very different from monometallic gold. These results provide a clear evidence of a synergetic effect between gold and copper. The samples containing more copper (1:0.7, 1:0.9, and 1:1.2) show rather close conversion. In the following, the Au:Cu 1:0.9 catalyst was used to study the influence of the temperature of activation in air, from 250 to 500 °C. Fig. 1b shows that pretreatment at 300 °C in air leads to the most active catalyst.

Fig. 2a shows the CO conversion as a function of the reaction temperature for the Au–Cu/TiO_2 catalysts after activation under hydrogen at 200 °C. Activation under hydrogen leads to less active catalysts than activation in air (Fig. 1a) and to catalysts less active than monometallic Au/TiO_2. At reaction temperature higher than 100 °C, the Au–Cu/TiO_2 catalysts become slightly more active than monometallic Au/TiO_2. The Cu/TiO_2 sample was completely inactive in the whole temperature reaction range (0–200 °C). Fig. 2b shows that 200 °C is the optimal activation temperature under hydrogen for Au–Cu 1:0.9.

As the Au–Cu catalysts activated in air are more active than the ones activated in hydrogen, some of them were submitted to CO + O_2 stream for 24 h at 20 °C in order to determine their stability. Fig. 3 compares the results obtained for Au/TiO_2, Au:Cu 1:0.9 and Au:Cu 1:1.2 catalysts activated in air at 300 °C: whereas Au/TiO_2

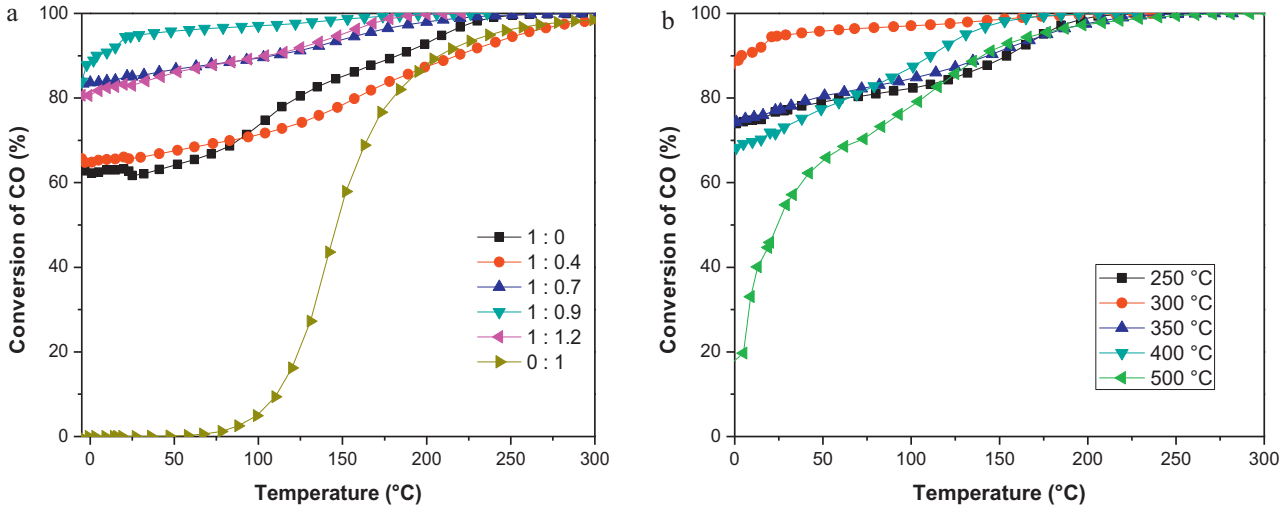

Fig. 1. CO oxidation light-off curves of (a) monometallic Au and Cu and bimetallic Au–Cu catalysts activated at 300 °C in air, (b) Au–Cu 1:0.9 catalyst as a function of the temperature of activation in air. Reaction conditions: 40 mg of pure catalyst, 100 mL min^{-1} of CO 1%, O_2 1% balanced N_2.

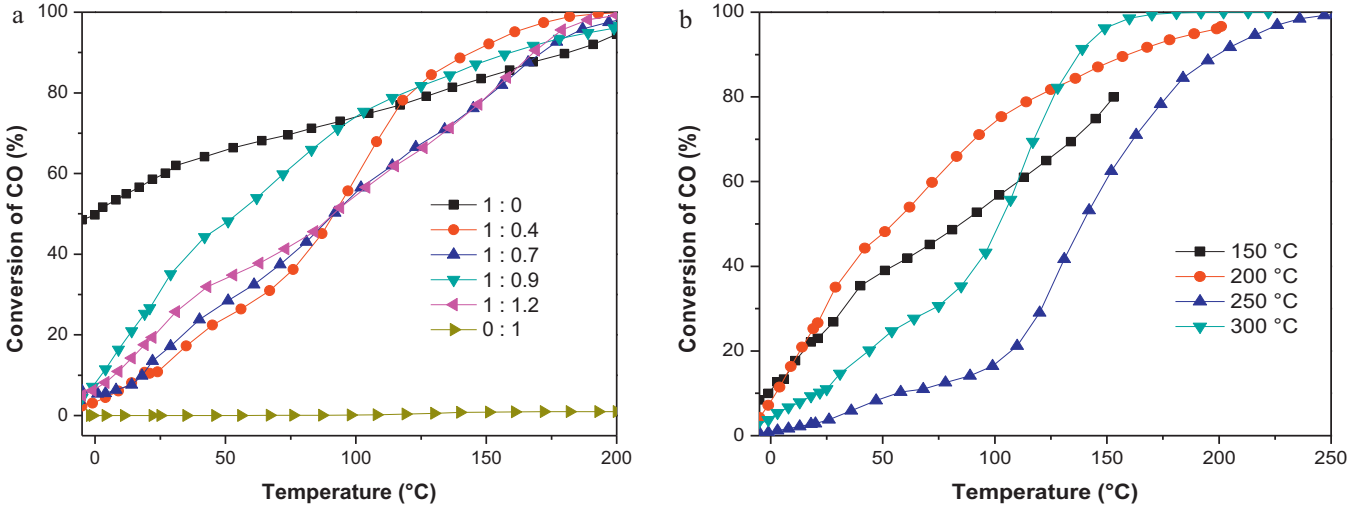

Fig. 2. CO oxidation light-off curves of (a) monometallic Au and Cu and bimetallic Au–Cu catalysts activated at 200 °C in hydrogen, (b) Au–Cu 1:0.9 catalyst as a function of the temperature of activation in hydrogen. Reaction conditions: 40 mg of pure catalyst, 100 mL min^{-1} of 1% CO, 1% O_2 balanced N_2.

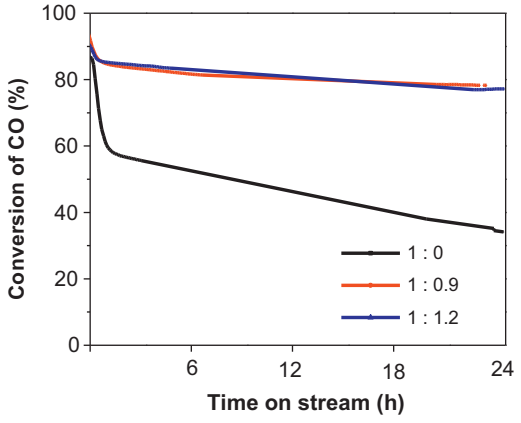

Fig. 3. Evolution of conversion of CO (%) as a function of time on stream at 20 °C for the Au/TiO_2, Au–Cu 1:0.9 and Au–Cu 1:1.2 catalysts activated in air at 300 °C. Reaction conditions: 40 mg of pure catalyst, 100 mL min^{-1} of 1% CO, 1% O_2 balanced N_2.

deactivates continuously during the 24 h on-stream and loses 62% of the initial activity, the bimetallic Au:Cu 1:0.9 and Au:Cu 1:1.2 catalysts are much more stable since they lose less than 15% of the initial activity. Hence, the addition of Cu to Au catalysts leads to more stable catalysts than the monometallic gold one.

As shown in Table 2, the Au:Cu 1:0.9 catalyst is more active than Au/TiO_2 at 30 °C (results obtained in kinetic regime). The reaction rate (0.015 mol mol^{-1} Au s^{-1}) is almost 4 times higher than that of Au/TiO_2 tested in the same reaction conditions, and the TOF is also almost 3 times higher. Table 2 also shows that the reaction rate of our Au–Cu catalysts is very close to those previously reported of $Au–Cu/TiO_2$ and $Au–Cu/SiO_2$ for similar reaction temperatures and particle size [26,36]. Let us note that after calcination, Cu is in the form of CuO_x and, as proposed in Sections 4.3 and 4.4, Au can be deposited on CuO_x; because of this, the average particle size measured by TEM must correspond to the one of Au.

Fig. 4 reports the Arrhenius plots obtained by diluting the Au/TiO_2 and Au–Cu 1:0.9 catalysts, obtained between 20 and 80 °C, *i.e.*, at conversions lower than 15%. As shown in Fig. 4, the apparent activation energy of the Au–Cu 1:0.9 catalyst is 19 kJ/mol, whereas the one of Au/TiO_2 was 35 kJ/mol. The latter is similar to the

Table 2
Comparison of the reaction rates for the CO oxidation of Au–Cu/TiO_2 catalysts with those reported in the literature. The determination of the reaction rate at 30 °C was performed in kinetic regime using a dilution of 60% of catalyst in TiO_2 (see Section 2.2).

Catalyst	T (°C)	Av. particle size (nm)	Contact time (g_{cat} hmol^{-1} CO)	Reaction rate (mol mol^{-1} Au s^{-1})	TOF (s^{-1})	Source
Au/TiO_2	30	3.2	9.6	0.004	0.01	This work
Au–Cu 1:0.9	30	2.7	9.6	0.015	0.029	This work
$Au_{20}Cu_1/SiO_2$	30	3.6	4.3	0.011	0.036	[26]
Au–Cu/TiO_2	25	3–4	–	0.015	–	[36]

values reported in the literature for Au/TiO_2 catalysts prepared by the deposition–precipitation method [45]. The apparent activation energy of the Au–Cu 1:0.9 catalyst is about half of the activation energy of the Au/TiO_2 catalyst. The difference is discussed later in Section 4.4.

To attempt to explain the catalytic results, characterizations were performed on the series of bimetallic samples and for the Au:Cu 1:0.9 sample after different activation temperatures. Comparisons are made with monometallic samples.

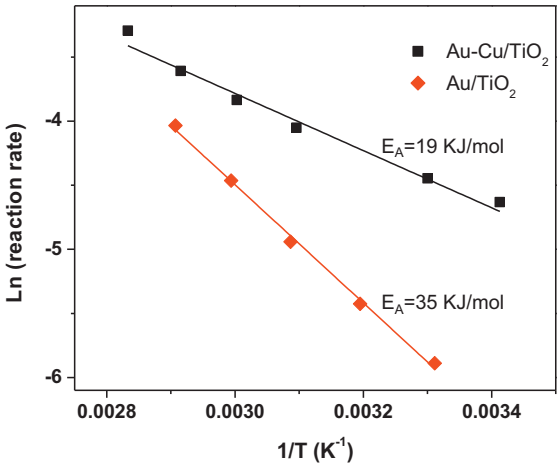

Fig. 4. Arrhenius plots of the temperature dependence of Au/TiO_2 and Au:Cu 1:0.9 catalysts. Reaction conditions: catalyst diluted to 60% (24 mg of catalyst + 16 mg of TiO_2), 100 mL min^{-1} of 1% CO, 1% O_2 balanced N_2.

3.3. Reducibility of gold and copper in the dried samples

3.3.1. TPR characterization

The reducibility of the dried samples was studied by TPR. Fig. 5A displays the TPR profiles of Au/TiO_2, Cu/TiO_2 and the bimetallic Au–Cu/TiO_2 samples. In the case of Au/TiO_2, the reduction profile appears as a single peak between 100 and 160 °C with a maximum at 120 °C. For Cu/TiO_2, the maximum of the peak was observed at 160 °C (140–185 °C). These results show that Au and Cu were still in the oxidized form after drying, and that they were reduced at 120 and 160 °C, respectively. For the bimetallic samples, the reduction profile was also characterized by a single peak with a maximum that shifted from 133 to 154 °C when the Cu content was increased in the sample, *i.e.*, between the temperature of reduction of gold and the one of Cu. Moreover, the temperatures at which reduction started and terminated were also shifted to higher temperatures when the Cu content was increased in the sample. These low temperature peaks have been assigned to the reduction of Au^{3+} [46,47] and Cu(II) oxide [30,48] species. A second broad reduction peak at temperatures higher than 300 °C was observed in Cu/TiO_2. This peak shifted to lower temperatures for the Au:Cu catalysts. Such a broad reduction peak has been ascribed to the reduction of CuO particles having little or no interaction with the support [49].

In order to determine the oxidation state of Cu in the Au:Cu catalysts after calcination at 300 °C and after CO oxidation, TPR of Au:Cu 1:0.9 was performed (shown by profiles b and c of Fig. 5B, respectively). The TPR profile of Au/TiO_2 calcined at 300 °C before and after reaction did not show reduction peaks, indicating that gold was completely reduced (this profile is not shown). These results are in agreement with previous XANES results on Au/TiO_2 catalysts prepared by the same method and calcined at the same temperature [50]. The reduction peak observed at about 170 °C (140–195 °C)

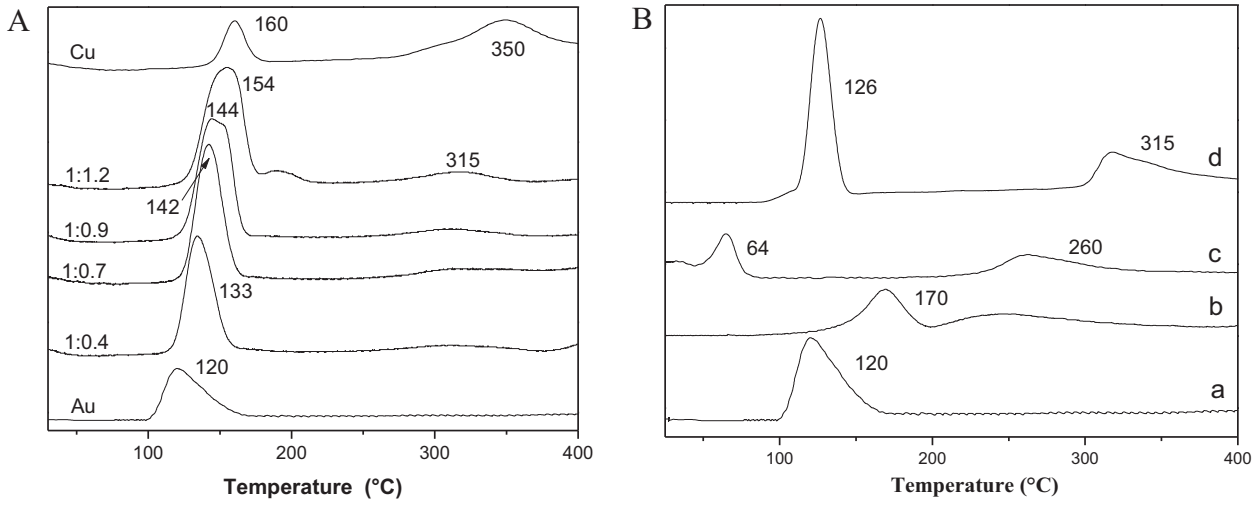

Fig. 5. (A) TPR profiles of dried monometallic Au/TiO_2 and Cu/TiO_2 and bimetallic Au–Cu catalysts with various Au/Cu ratios. (B) TPR profiles of (a) dried Au/TiO_2, (b) Au–Cu 1:0.9 after calcination at 300 °C, (c) calcined Au–Cu 1:0.9 after CO oxidation reaction, and (d) Cu/TiO_2 after calcination at 300 °C.

Table 3
Hydrogen consumption during TPR of the monometallic and bimetallic Au:Cu samples after drying or calcination.

Sample	Theoretical hydrogen consumption [mmol g^{-1}]	Experimental hydrogen consumption [mmol g^{-1}]	[Experimental consumption]/[theoretical consumption]
Au	0.0145	0.0126	0.88
Cu	0.0095	0.0099	1.04
Cu after calcination at 300 °C	0.0094	0.0137	1.4
Au:Cu 1:0.4	0.0187	0.0185	0.99
Au:Cu 1:0.7	0.0208	0.0185	0.90
Au:Cu 1:0.9	0.0235	0.0223	0.95
Au:Cu 1:1.2	0.02878	0.0279	0.97
Au:Cu 1:0.9 after calcination at 300 °C	0.0091[a]	0.0087	0.96
Au:Cu 1:0.9 after calcination and CO oxidation	0.0091[a]	0.0078	0.86

[a] Considering the Cu loading only, *i.e.*, considering that gold was fully reduced.

in the TPR profile of Au:Cu 1:0.9 after calcination (Fig. 5Bb) must therefore be due to the reduction of Cu species. The TPR profile of Au:Cu 1:0.9 after CO oxidation (Fig. 5Bc) shows a reduction peak at 65 °C that must also be due to the reduction of Cu species. However, it can be noted that this peak appears at much lower temperature than that of calcined Au:Cu 1:0.9. For comparison, the TPR profile of dried Au/TiO_2 (Fig. 5Ba) and monometallic Cu/TiO_2 samples calcined at 300 °C (Fig. 5Bd) are also shown.

For the fresh monometallic and bimetallic samples, quantitative measurements of the H_2 consumption during the TPR experiments, characterized by the ratio of the [experimental H_2 consumption]/[theoretical consumption] (Table 3), showed that the experimental H_2 consumption values were close to the stoichiometric value expected for the Au^{3+} or Cu^{2+} reduction process taking into account the gold and copper loadings determined by ICP analysis.

For the samples calcined at 300 °C in air, the consumption of H_2 for the monometallic Cu/TiO_2 sample was slightly higher than the stoichiometric value, whereas for Au/TiO_2, the H_2 consumption was null, indicating that gold was completely reduced after calcination at 300 °C. For the bimetallic Au:Cu 1:0.9 sample H_2 consumption indicated that copper was completely oxidized after calcined at 300 °C and also after CO oxidation.

In summary, after calcination, gold was totally reduced and copper was oxidized, whereas after reduction at 200 °C, which was the optimal activation temperature for CO oxidation (Fig. 2b), gold was fully reduced, and copper was only partially reduced. The complete reduction of Cu was reached at temperatures near 300 °C.

3.3.2. UV–vis characterization

The UV–vis spectra of the Au/TiO_2, Cu/TiO_2 and Au–Cu 1:0.9 samples were recorded during *in situ* reduction under hydrogen between RT and 300 °C (Fig. 6A). All the samples developed a broad band between 400 and 800 nm that increased in intensity as the reduction temperature increased. The band centered at ~530 nm for Au/TiO_2 (Fig. 6Aa) and at ~580 nm for Cu/TiO_2 (Fig. 6Ab) is due to the surface plasmon resonance (SPR) of metallic gold and copper, respectively [51–53]. The absorption band of Au–Cu 1:0.9 presented a maximum at ~570 nm (Fig. 6Ac). It is interesting to note that whereas at 180 °C the SPR band of Cu in Cu/TiO_2 and Au in Au/TiO_2 was already completely developed, its formation was delayed in Au–Cu 1:0.9; it started to become visible above 180 °C and evolved up to 240 °C. These differences in the temperature of appearance of SPR between the monometallic and the bimetallic samples may indicate that the absorption band is not the mere summation of the SPR of Cu and Au, but it might result from the interaction of Au with Cu species. The TPR (Fig. 5) and UV–vis results (Fig. 6) also confirm that gold and copper species were in an oxidized state in the dried samples (Au, Cu and Au–Cu).

The UV–vis spectra of Au/TiO_2, Cu/TiO_2 and Au–Cu 1:0.9 samples were also recorded during *in situ* calcination under air from RT to 300 °C (Fig. 6B). The Au/TiO_2 and Au–Cu samples developed a SPR band (Fig. 6Ba and c), whereas the Cu/TiO_2 sample did not (Fig. 6Bb), which indicates that Cu remained as copper oxide in the monometallic sample. The plasmon band in the calcined Au/TiO_2 sample (Fig. 6Ba) was centered at about 550 nm, *i.e.*, was slightly shifted compared to the reduced sample (maximum at 530 nm, Fig. 6Aa). Moreover, the temperature at which the gold plasmon band appeared in calcined Au/TiO_2 (220 °C) and the temperature at which the maximum intensity was reached (300 °C) (Fig. 6Ba) was delayed compared to the reduced sample (140 and 180 °C, respectively, Fig. 6Aa). This confirms former results that reduction of Au is slower in air than in hydrogen [54,55]. The differences in the plasmon band position and intensity as a function of the atmosphere of activation can be explained by the different size or shape of the gold particles [52]. It is well known that gold nanoparticles are smaller after reduction than after calcination at the same temperature [42,55]; this is shown in the next section.

3.4. Size and composition of the nanoparticles after activation

Fig. 7 shows typical HAADF images of Au–Cu 1:0.9 activated in air at 200, 300, 400 and 500 °C. The average metal particle size increased with temperature from 2.4 nm to 5.6 nm (Table 4). The same trend was observed when the Au–Cu sample was activated in H_2, but the particles seemed slightly smaller (Table 4). Table 5 reports the metal particle size in the Au–Cu catalysts with different Cu/Au ratios after activation at 300 °C in air or at 200 °C in hydrogen. The average particle sizes of the calcined samples were slightly smaller, between 2.4 and 2.9 nm, than the ones in Au/TiO_2 (3.2 nm). The samples activated in hydrogen led to slightly smaller particles (between 2.0 and 2.5 nm, Table 5). Let us note that it was not possible to observe Cu particles in calcined or reduced Cu/TiO_2 because of the lack of contrast between Cu and Ti.

In order to determine the composition of the particles in the bimetallic samples, about 40 individual particles were randomly analyzed by micro EDS in calcined and reduced Au–Cu 1:0.90 samples. Because of the limited sensitivity of the technique, EDS could not be performed on particles smaller than 2 nm. It is important to remember that these analyses were not quantitative (see Section 2.3) and to note that both Au and Cu were detected in all particles (Table 4 and Fig. 8). The micro-EDS analysis of the Au–Cu 1:0.9 catalyst as a function of the activation temperature showed that when the activation temperature increased (under H_2 or air), the Cu/Au ratio decreased (Table 4), and so did the dispersion of the Cu/Au values (Fig. 8a and b), *i.e.*, the composition of the particles became more homogeneous. The difference between the measured Cu/Au ratio by EDS and the actual ratio (1:0.9) could be due to the fact that in most of the samples the smallest particles (<2 nm) could not be analyzed because of the too weak signal of XRD reaching the detector of the STEM microscope. It can be inferred that the

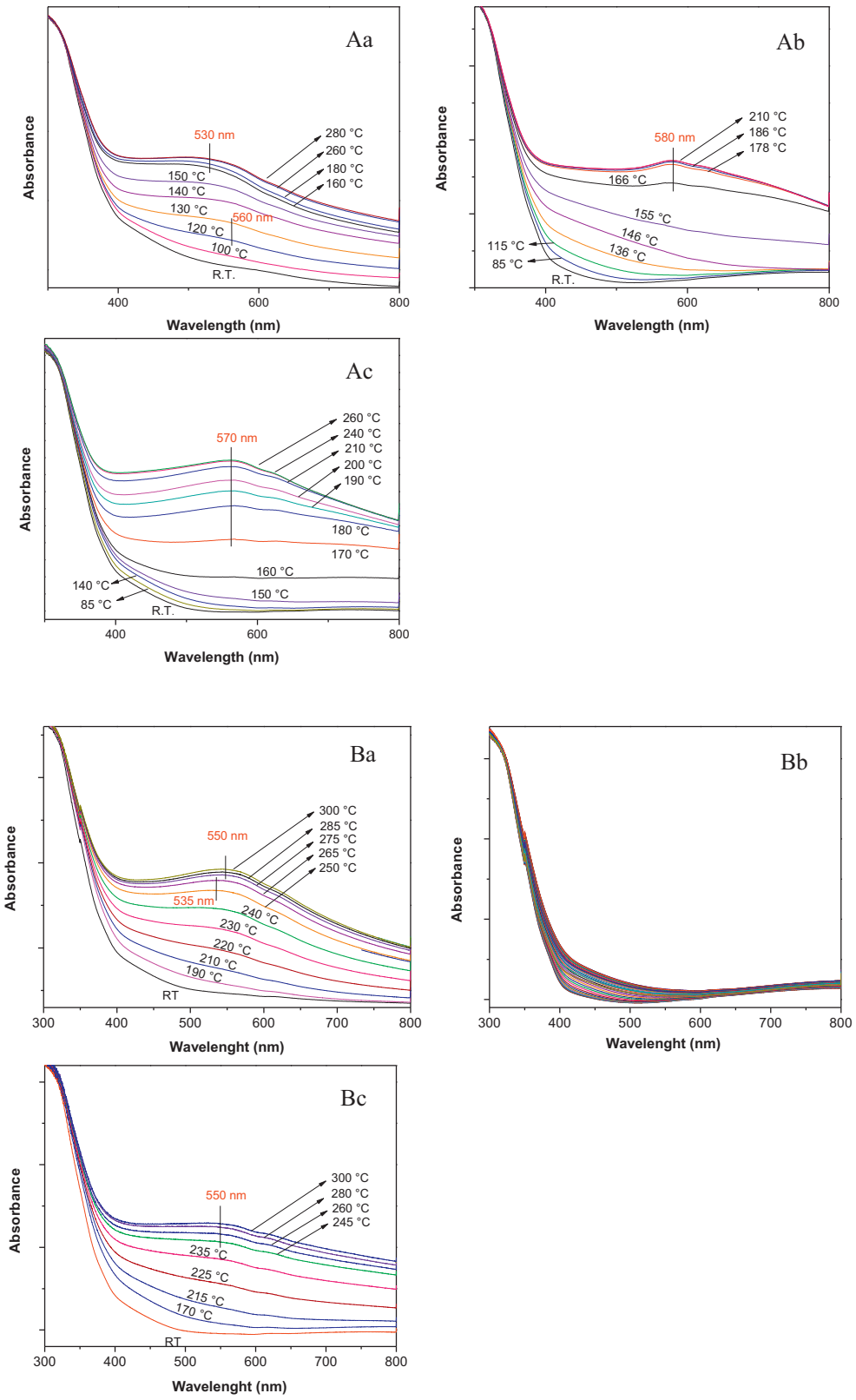

Fig. 6. UV–vis spectra of samples reduced *in situ* under hydrogen at increasing temperatures (Spectra A) and calcined *in situ* under air at increasing temperatures (Spectra B) for the (a) Au/TiO_2, (b) Cu/TiO_2, and (c) Au–Cu 1:0.9 samples.

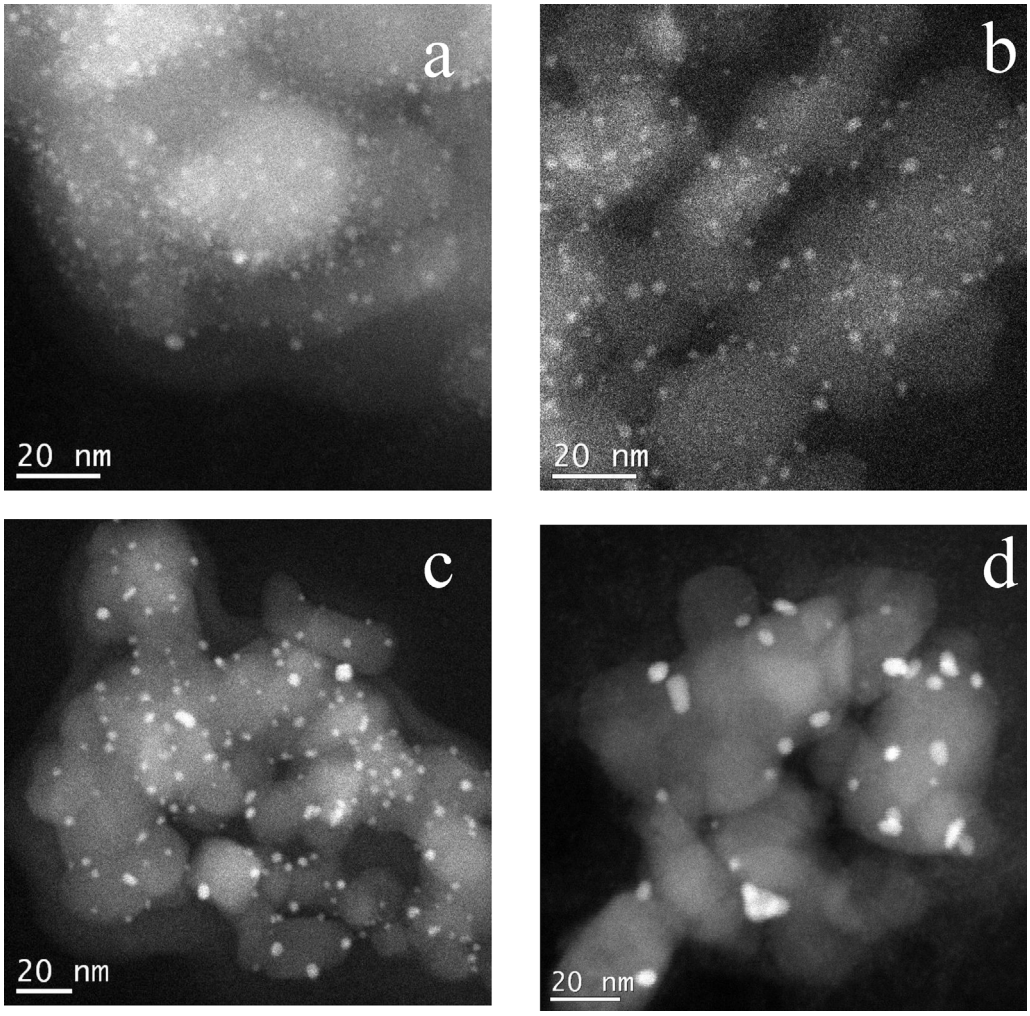

Fig. 7. HAADF images of the Au–Cu 1:0.9 catalyst after different temperatures of activation in air: (a) 200 °C, (b) 300 °C, (c) 400 °C, and (d) 500 °C.

Table 4
Evolution of the average particle size and particle composition (determined by micro-EDS) in catalyst Au–Cu 1:0.9 as a function of the activation temperature in air and in hydrogen.

Activation gas	Temperature of activation	Average particle size (nm)	Standard deviation (nm)	Cu/Au atomic ratio
Air	200 °C	2.4	0.46	6.0
	300 °C	2.7	0.58	5.3
	400 °C	3.2	0.75	1.5
	500 °C	5.6	1.3	1.2
Hydrogen	150 °C	1.9	0.50	15.0
	200 °C	2.2	0.66	10.0
	300 °C	2.5	0.71	3.9

Table 5
Average particle size in Au–Cu catalysts with various Au/Cu atomic ratios, activated in air at 300 °C or in hydrogen at 200 °C.

Catalyst	Activated in air		Activated in hydrogen	
	Average particle size (nm)	Standard deviation (nm)	Average particle size (nm)	Standard deviation (nm)
Au/TiO_2	3.2	0.84	2.5	0.74
Au–Cu 1:0.4	2.9	0.78	–	–
Au–Cu 1:0.7	2.4	0.66	2.5	0.79
Au–Cu 1:0.9	2.7	0.58	2.2	0.51
Au–Cu 1:1.2	2.2	0.54	2.0	0.41

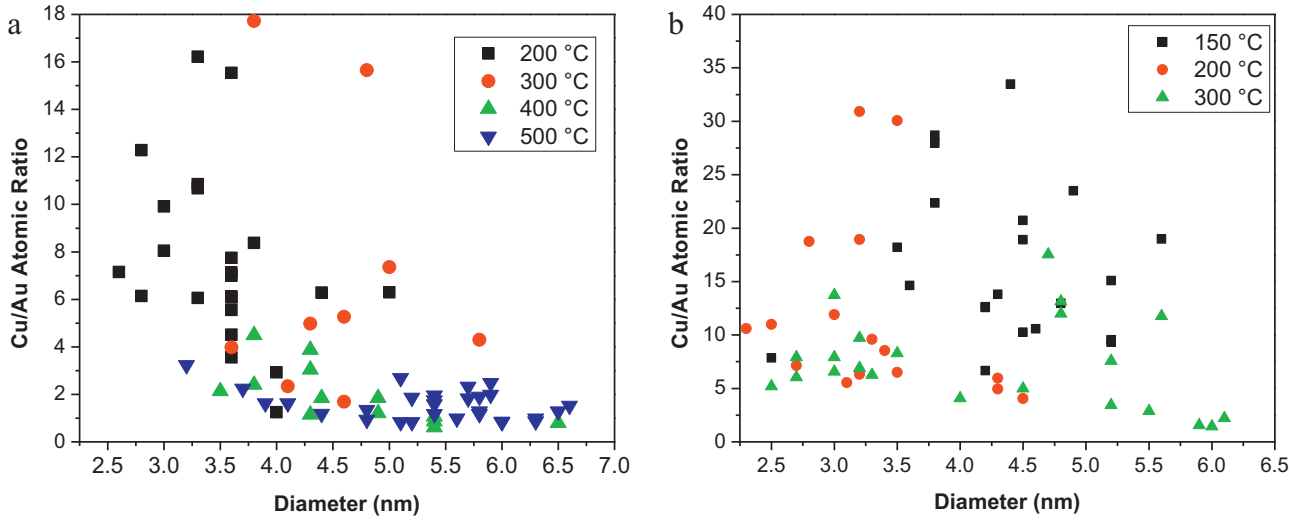

Fig. 8. Cu/Au atomic ratios of individual particles obtained by micro-EDS for Au–Cu 1:0.9 catalysts as a function of the temperature of activation: (a) in air and (b) in H_2.

smallest particles (which could not be analyzed) contain a higher proportion of gold. Some of these results will be discussed later.

3.5. Surface composition of the catalysts by CO-DRIFTS

To investigate the surface composition of the particles in Au–Cu/TiO_2, CO adsorption was studied on the Au–Cu 1:0.9 sample by DRIFTS after *in situ* activation in hydrogen at 200 °C or air at 300 °C, and compared with the monometallic Au and Cu samples.

3.5.1. Reduced samples

The introduction of CO at room temperature in Au/TiO_2 reduced at 200 °C led to the immediate appearance of one carbonyl band at 2101 cm^{-1} (Fig. 9a) that can be attributed to CO adsorbed on low coordinated surface Au^0 atoms [56,57]. However, under the CO flow at RT, this band remained almost constant, whereas a new band around 2074 cm^{-1} and a shoulder around 2000 cm^{-1} appeared and increased. The band at 2074 cm^{-1} has been assigned to negatively charged gold carbonyls [57–59], resulting from the creation of new sites of adsorption due to the reconstruction of the gold nanoparticles under CO [60].

Heating the sample in CO atmosphere at temperatures up to 200 °C induced a gradual decrease in intensity of all bands without complete disappearance, accompanied by a shift of the band at 2074 cm^{-1} to lower frequencies (2032 cm^{-1}) (Fig. 9b). This red shift can be attributed to the decrease of the CO dipole–dipole interaction because of the decreasing CO coverage of the gold particles as temperature increases [60].

The adsorption of CO on reduced Cu/TiO_2 (Fig. 9c) led to the appearance of an intense band at 2062 cm^{-1} attributed to Cu^0–CO [61], a shoulder at 2000 cm^{-1}, and a broad band centered at about 1900 cm^{-1}. Bands between 2000 and 1900 cm^{-1} have been attributed to bridged CO species on Cu^0 [62,63]. The broad band at 1900 cm^{-1} has been also observed [64,65] on Cu(I)Y zeolite in spectra recorded at 25 °C, and attributed to CO bridged on two Cu^+ species. According to these authors, they are among the few known bridging carbonyls formed on surface cation sites [65].

During heating up to 200 °C in CO atmosphere, the band at 2062 cm^{-1} slightly decreased and shifted to 2046 cm^{-1}, this shift is associated with the decrease in the coverage of CO (Fig. 9d), the shoulder at 2000 cm^{-1} decreased and disappeared, whereas the band at 1900 cm^{-1} increased. The decrease of the band at high wavenumbers with the increase in the band around 1900 cm^{-1} has been previously observed [63] and it has been proposed that this behavior is due to a reconstruction of the copper surface, which changes the adsorption sites of CO because of the increase of the temperature. It is important to note that the Cu/TiO_2 spectra were much less intense than the Au/TiO_2 spectra in spite of the same atomic loadings. Moreover, compared to Au/TiO_2, CO is more strongly bonded on Cu^0 than on Au^0, in agreement with the energy of adsorption obtained for Au/Al_2O_3 and Cu/Al_2O_3; 62 kJ/mol in CO adsorbed on Au^0 [60] and 82 kJ/mol in CO adsorbed on Cu^0 [63].

After admission of CO on the reduced Au–Cu 1:0.9 sample, two bands were observed, the first one centered at 2093 cm^{-1} attributed to Au^0–CO, and the second one centered at 2068 cm^{-1} attributed to Cu^0–CO as well as shoulders at around 2010 and 1900 cm^{-1} (Fig. 9e). They barely changed with time under CO. However, one can note that the band at 2093 cm^{-1} is slightly shifted compared to the one of the reduced monometallic Au/TiO_2 catalyst (Fig. 9a), and that the band at 2068 cm^{-1} as also slightly shifted compared to that of the reduced Cu/TiO_2 (Fig. 9c).

When the Au–Cu catalyst was heated under CO up to 200 °C (Fig. 9f), the band of Au^0–CO at 2093 cm^{-1} gradually decreased and disappeared as for Au/TiO_2 (Fig. 9b), whereas the band at 2068 cm^{-1} shifted to 2048 cm^{-1} and increased, which was not observed in reduced Cu/TiO_2 (Fig. 9d); the broad band at 1900 cm^{-1} increased as in reduced Cu/TiO_2. The spectra obtained at temperatures higher than 100 °C were very similar to those of the Cu/TiO_2 catalyst. This last fact may indicate that when the temperature increases, copper atoms migrate to the surface of the particles.

3.5.2. Calcined samples

The same DRIFTS study was performed after *in situ* calcination in air at 300 °C (Fig. 10). For the Au/TiO_2 catalysts, the introduction of CO (Fig. 10a) led first to the appearance of a band at 2107 cm^{-1} attributed to CO adsorbed on Au^0 [56,57]. This band transformed in the band of $Au^{\delta-}$–CO (2075 cm^{-1}) as in the case of the reduced samples (Fig. 9a), but much more slowly. A shoulder was also observed, but at slightly higher frequency around 2015 cm^{-1} instead of around 2000 cm^{-1} (Fig. 9a); however, its assignment is uncertain. This band has been once observed [60] and on the basis of DFT calculation [66], it has been assigned to bridged CO species on metal gold atoms although gold is not known to bridge CO.

When the sample was heated in CO atmosphere, the band at 2075 cm^{-1} decreased before disappearing at 300 °C (Fig. 10b). The smaller band around 2100 cm^{-1} also decreased in intensity, but it seemed to disappear at lower temperature. As for the reduced

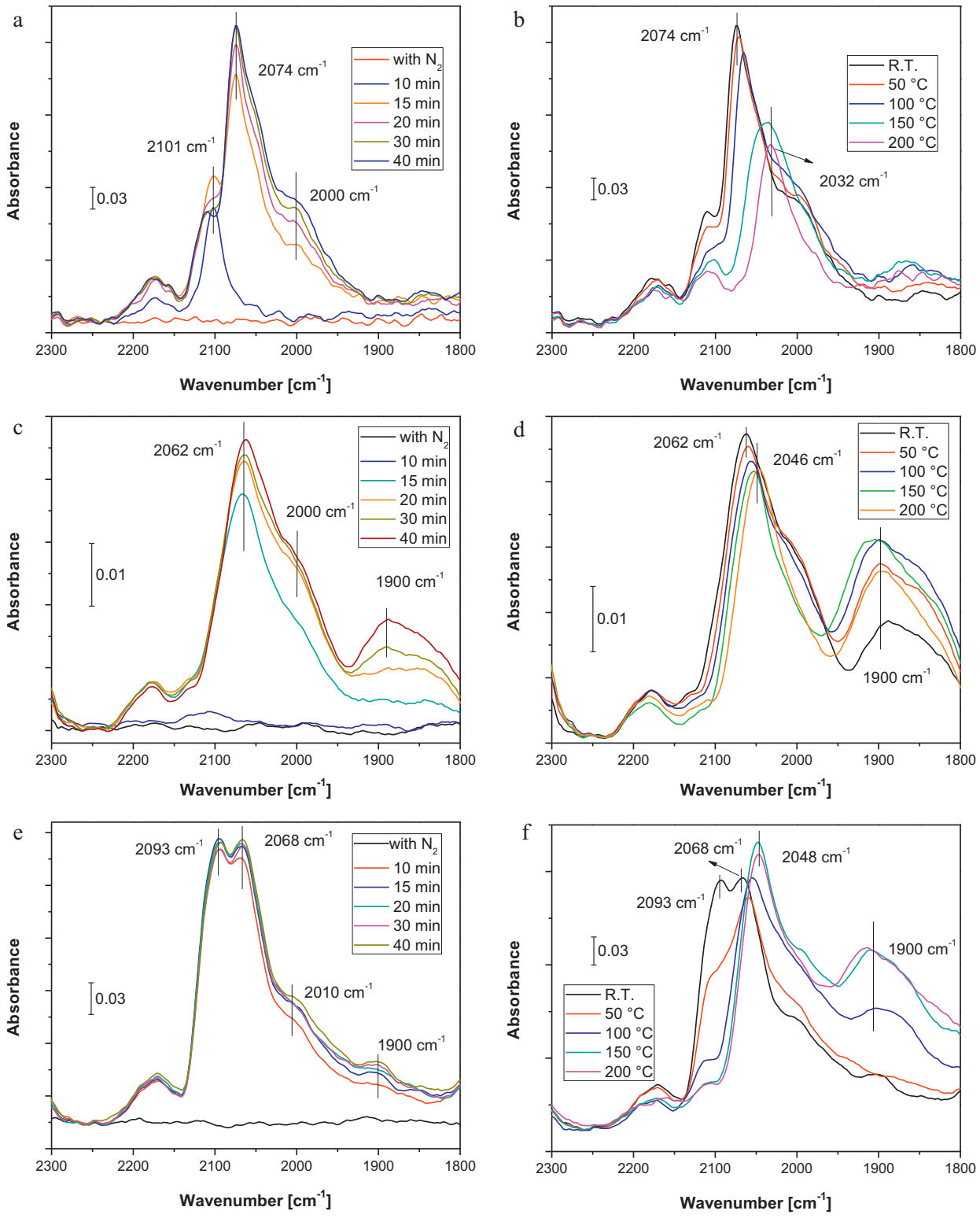

Fig. 9. DRIFT spectra of CO adsorbed on (a) and (b) Au/TiO_2; (c) and (d) Cu/TiO_2; (e) and (f) Au:Cu 1:0.9 catalysts, all of them activated in hydrogen at 200 °C.

sample, the decrease of the band at 2075 cm^{-1} was accompanied by a shift to lower frequencies (Fig. 9b).

The adsorption of CO on calcined Cu/TiO_2 (Fig. 10c) led to the appearance of an intense band at 2106 cm^{-1} attributed to Cu^+–CO [61,67], and of a weak one at 2060 cm^{-1} corresponding to Cu^0–CO [61]. As in the reduced samples, the intensity of the bands of Cu/TiO_2 calcined samples was weaker compared to the intensity of the bands of Au/TiO_2 calcined sample. Both bands increased under CO without band shift. It has been reported that CO poorly adsorbs on Cu^{2+} [65] and that Cu^{2+} can be reduced to Cu^+ by CO at RT [67]. Heating Cu/TiO_2 in CO atmosphere at temperatures up to 150 °C resulted in an increase in the intensity of the band of Cu^+–CO and of Cu^0–CO (Fig. 10d), probably resulting from further reduction of oxidized copper. Between 150 and 300 °C, the intensity of both bands decreased because of the shift in the equilibrium of CO adsorption–desorption. However, at 300 °C, the Cu^+–CO band was

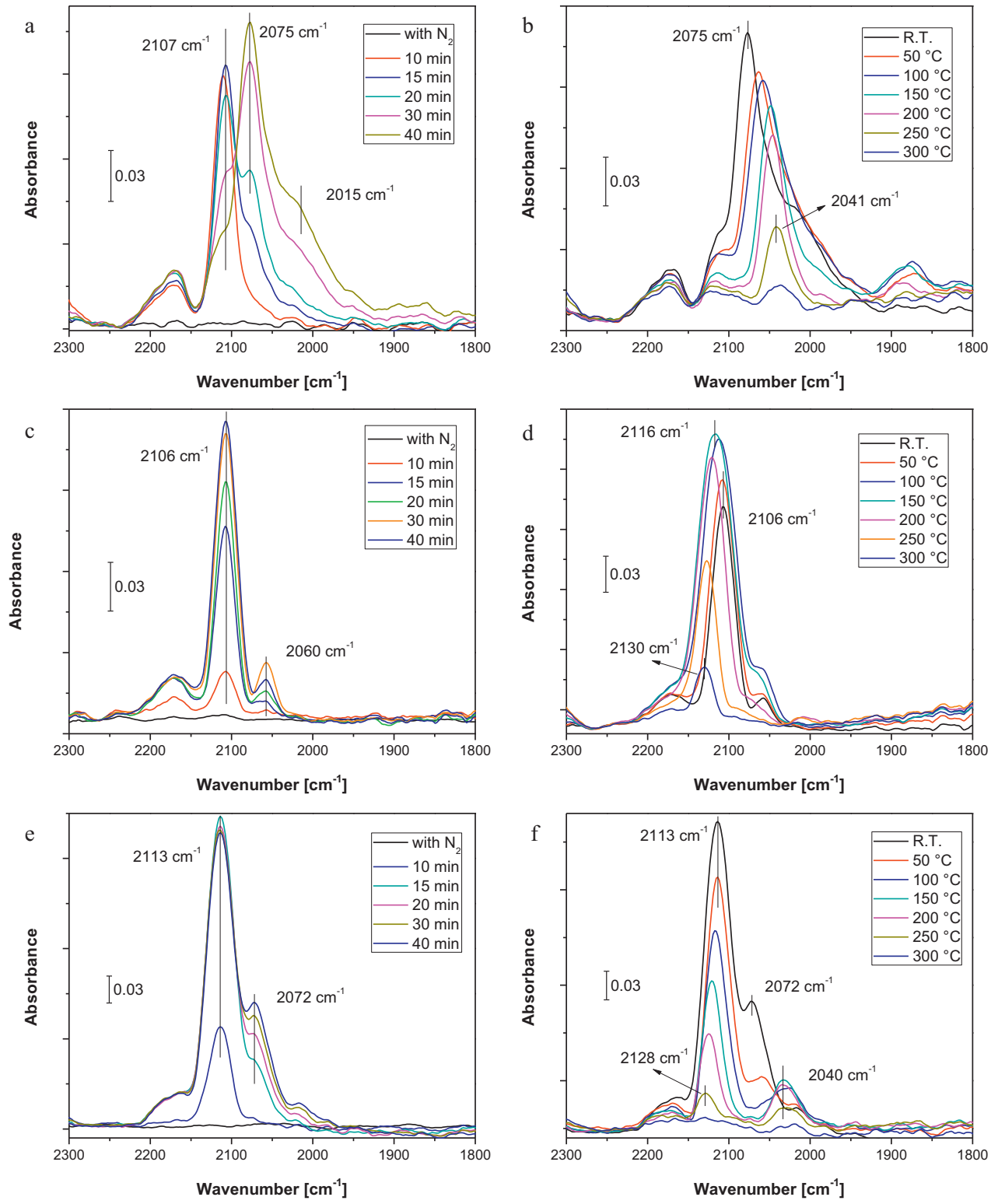

Fig. 10. DRIFT spectra of CO adsorbed on the following catalysts: (a) and (b), Au/TiO_2: (c) and (d), Cu/TiO_2; and (e) and (f), Au:Cu 1:0.9. All of them activated in air at 300 °C.

still observed but shifted to 2130 cm^{-1}, whereas that of Cu^0–CO had disappeared.

In the case of the calcined Au–Cu 1:0.9 sample, after admission of CO in the cell (Fig. 10e), a band at 2113 cm^{-1} appeared. According to the reference spectra (Fig. 10a and c), it may have resulted from the sum of the contributions of the Au^0–CO (2107 cm^{-1}) and Cu^+–CO bands (2106–2116 cm^{-1}). Under CO contact at RT, the band at 2072 cm^{-1} attributed above to $Au^{\delta-}$–CO (2075 cm^{-1}), appeared and increased in intensity as in the case of Au/TiO_2, calcined (Fig. 10a) or reduced (Fig. 9a), whereas the intensity of the band at 2113 cm^{-1} remained almost constant. This is a confirmation of the TPR results (Fig. 5B) that showed that gold was in reduced form and that Cu was in oxidized form in the calcined bimetallic catalysts. Heating the Au–Cu 1:0.9 sample in CO atmosphere at

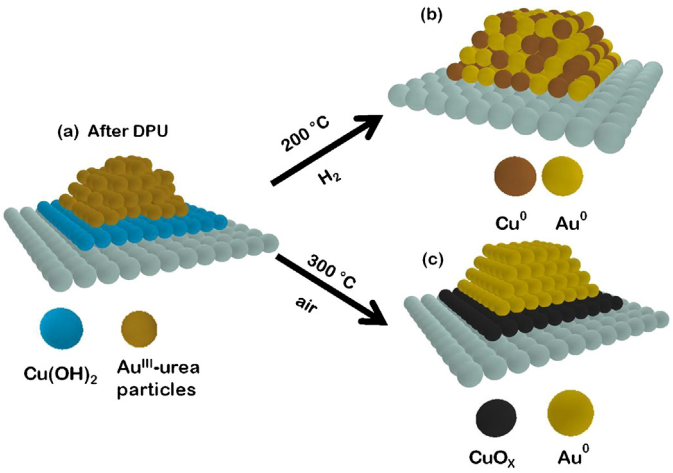

Scheme 1. Evolution of the structure of the bimetallic catalyst after drying (a), activated in hydrogen (b), and activated in air (c).

temperatures up to 300 °C resulted in a decrease of the intensity of the bands at 2113 cm^{-1} and 2072 cm^{-1} (Fig. 10f). These decreases were accompanied by a shift of the band at 2113 to 2128 cm^{-1} and by the appearance of a new band at 2040 cm^{-1}, which could correspond to a $Au^{\delta-}$–CO, by analogy with the spectra of calcined Au/TiO_2 (Fig. 10b). Unlike Cu/TiO_2, for the Au–Cu 1:0.9 sample at 300 °C, the band at 2128 cm^{-1} had disappeared.

4. Discussion

4.1. Dried samples

The appearance of reduction peaks in the TPR profiles (Fig. 5) and the absence of SPR absorption bands in the first UV–vis spectra before thermal treatment, *i.e.*, after drying (Fig. 6A and B) indicate that both gold and copper were in oxidized state after preparation and drying, whether they were in monometallic or bimetallic samples.

According to former studies, copper is deposited onto the support as a copper hydroxide during deposition–precipitation with urea [44] and gold as a gold–urea compound [40]. For the Au–Cu samples, one can anticipate that gold, which is deposited after copper deposition, deposits preferentially on copper hydroxide rather than on titania. Indeed, the point of zero charge of $Cu(OH)_2$ and CuO is about 9.5, whereas the one of TiO_2 was about 6.5 [68]. The Au species, negatively charged at the beginning of DPU ($AuCl_4^-$ or $AuOHCl_3^-$) [40], can preferentially interact with $Cu(OH)_2$ forming a Au/CuO system supported on TiO_2 (Scheme 1a). It is well known that deposition–precipitation is effective only for the deposition of gold on oxides with IEP higher than ~4 [40]. This is not true for copper (which gives cationic complexes), and there are papers showing that copper can be deposited on silica (IEP lower than 3) by deposition–precipitation with urea [69]. As the Au species negatively charged can preferentially interact with $Cu(OH)_2$ forming a Au/CuO system, this method of sequential deposition–precipitation of copper first and gold second should also be effective to prepare Au–Cu on SiO_2.

4.2. Reduced samples

As mentioned above, after thermal treatment under hydrogen at 200 °C, gold was in the metallic state, whereas copper was only partially reduced in the monometallic samples. This was attested by the presence of plasmon resonance absorption (Fig. 6Aa, b) and of IR bands at 2101 cm^{-1} for Au/TiO_2, and at 2062 cm^{-1} (Cu^0) and a shoulder at 2106 cm^{-1} (Cu^I) for Cu/TiO_2 (Fig. 9a and c) after reduction at 200 °C. TPR and UV–vis spectroscopy also showed that gold was reduced at a lower temperature (<120 °C) than copper (reduction peaks at 160 and 350 °C) (Figs. 5A and 6Ac). In the case of the bimetallic system, a first TPR peak appeared between 100 and 180 °C, and a second broad and low intensity peak was observed at about 315 °C (Fig. 5A). Hence, after reduction at 200 °C, which is the optimal activation temperature for CO oxidation (Fig. 3b), Au was metallic and Cu was partially reduced. In agreement with this, the UV–vis spectra (Fig. 6Ac) showed that the plasmon band still increased in intensity above 200 °C.

According to TPR and DRIFTS, Au–Cu alloy particles may have formed upon reduction: (i) the TPR profiles of the bimetallic samples (Fig. 5A) were not the superimposition of those of Au/TiO_2 and Cu/TiO_2, (ii) the DRIFT spectra of the reduced bimetallic sample showed bands of Au^0–CO and Cu^0–CO at 2093 and 2068 cm^{-1}, respectively (Fig. 9e), shifted compared to those of the monometallic samples, 2101 and 2062 (Fig. 9a and c). Gold and copper, which have the same face-center cubic (fcc) crystal structure and similar lattice spacing, are known to form alloys very easily [70,71].

If the TPR profiles of each monometallic sample (Fig. 5A) are compared to their SPR absorption (Fig. 6Aa and b), it can be seen that the temperatures of beginning and end of reduction in hydrogen were roughly the same. This is not true for the bimetallic Au–Cu 1:0.9 sample since the temperatures of appearance and evolution of the plasmon band (Fig. 6Ac) were shifted to higher temperatures compared to the TPR profile (Fig. 5A). The reason for that may be that if gold is in contact with copper and forms alloy particles, the appearance and evolution of the SPR band may also be modified. Thus, the activation under hydrogen at temperatures near 300 °C causes the formation of Au^0–Cu^0 alloy particles, as shown in Scheme 1b.

4.3. Calcined samples

During calcination, only gold was reduced, whereas Cu remained in oxidized state. Indeed, the DRIFT spectrum of the calcined Au–Cu 1:0.9 sample recorded just after adsorption of CO (Fig. 10e) only shows the band at 2113 cm^{-1} corresponding to Au^0–CO and maybe to Cu^+–CO. Moreover, the UV–vis spectrum of Cu/TiO_2 remained flat and did not change during calcination (Fig. 6Bb), whereas SPR absorption appeared in the case of both Au/TiO_2 and $Au–Cu/TiO_2$ (Fig. 6Ba–c). The fact that the maximum of the reduction peak of calcined bimetallic $Au–Cu/TiO_2$ appeared at a lower temperature (Fig. 5Bb) than for Cu/TiO_2 (Fig. 5Bd) may attest for different reducibility of Cu, probably because of interaction with metallic gold. Several results are consistent with the hypothesis of an interaction between the gold particles and CuO (Scheme 1c): (i) the differences in the features of the plasmon band (broadness, intensity and energy) and the higher temperature at which it appeared for calcined Au–Cu (Fig. 6Bc) compared to Au/TiO_2 during reduction and calcination (Fig. 6Aa and Ba) could result from the formation of metallic gold particles in interaction with CuO_x. Indeed, the intensity and energy of the SPR band depend on the dielectric constant of the medium around the particles [72,73]. In the present case, the particle size of Au in Au/TiO_2 and in $Au–Cu/TiO_2$ was not very different (Table 5), but the dielectric constants of TiO_2 and CuO were different, and this influenced the SPR band energy. (ii) The point of zero charge of $Cu(OH)_2$ and CuO is higher than that of TiO_2 (see Section 4.1), during the preparation, gold would be preferentially deposited on Cu species. (iii) The fact that in the DRIFT spectra of calcined Au–Cu 1:0.9, the band at 2072 cm^{-1} of $Au^{\delta-}$–CO did not increase in intensity under CO at RT (Fig. 10e) as in the case of Au/TiO_2 (Fig. 10a) confirms the interaction between Au^0 and CuO. (iv) In all the particles analyzed by EDS,

both Au and Cu were detected. It can be observed that as the calcination temperature increased (Table 4), the Cu/Au ratio decreased; this may be due to the fact that concomitantly, the particle size increased. As the electron beam was 2 nm, understandably, a higher proportion of gold was detected when the particle size increased.

In summary, when the bimetallic samples were activated in air, gold was reduced and Cu remained in oxidized state forming Au^0–CuO_x/TiO_2 as shown in Scheme 1c. It is important to mention that copper was not detected by XRD on this sample, suggesting that CuO_x was amorphous or the particles were too small to be detected by XRD.

4.4. Catalytic properties of calcined and reduced Au–Cu samples

The differences in the chemical nature of the Au–Cu supported phase according to the nature of the pretreatment gas explain the different catalytic results, *i.e.*, that calcined Au–Cu samples produced more active and stable catalysts in CO oxidation catalysts than the reduced ones (Figs. 1b and 2b).

As mentioned above, the activation of Au–Cu samples under hydrogen produced less active catalysts than activation in air (Figs. 1a and 2b) and less active catalysts than Au/TiO_2 (Fig. 2a). Previous FTIR studies have shown that CO does not sufficiently adsorb onto Au–Cu alloy nanoparticles compared to Au nanoparticles [27]. This could be one of the reasons for the lower activity observed for the Au–Cu activated in hydrogen catalysts [27]. According to TPR, at 200 °C, Cu is not fully reduced; this could therefore explain why the catalyst activated in hydrogen at 200 °C was more active than those activated at higher temperatures. Fig. 6Ac also shows that the plasmon band still increased in intensity above 200 °C. The better activity of the reduced Au–Cu catalysts compared to monometallic Au/TiO_2 at reaction temperatures higher than 100 °C can be caused by the oxidation of copper due to the excess of oxygen present in the reaction flow. Indeed, the formation of a CuO_x/Au phase could be responsible for the enhanced activity shown by the reduced Au–Cu catalysts at reaction temperatures higher than 100 °C (Fig. 2a). This change from a Au–Cu alloy to CuO_x/Au in similar reaction conditions has been previously observed in alloyed Au–Cu/SBA15 systems [29] and in reduced Au–Cu/SiO_2 in a light off test [27]. The reduced catalyst was completely inactive at room temperature, it started to become active above 150 °C. It was shown by XRD and XAFS that, at this temperature, copper was segregated on the surface of the AuCu alloy and oxidized to form a Au–CuO composite structure, which was responsible for the activity [27].

As mentioned above, after reduction, the supported phase consisted of Au–Cu alloy nanoparticles supported on titania (Au^0–Cu^0/TiO_2) (Scheme 1b). The presence of Cu atoms on the particle surface attested by the IR bands of CO adsorbed on Cu had a negative effect on the catalytic properties of Au/TiO_2. The higher activity after activation in air, even at low temperature, in the temperature range where Cu/TiO_2 is completely inactive (<75 °C) indicates a synergetic effect between metallic gold and copper oxide. This is confirmed by the fact that the E_a value of the bimetallic catalyst was twice as low as that of Au/TiO_2 (Fig. 4) and the reaction rate of bimetallic Au–Cu catalysts was greater than that of Au/TiO_2 at 30 °C. The differences in E_a are somewhat difficult to interpret because the activation energy depends on intrinsic kinetic barriers, heats of adsorption, and relative surface coverages. However, the difference in the activation energy between the two samples is very large. Similar decreases in apparent activation energies compared to monometallic gold catalysts have been reported for bimetallic Au–Ni and Au–Pt catalysts tested in CO oxidation [74,75]. These differences indicate a substantial modification of the Au reactivity and validate the hypothesis that the gold particles interact with CuO particles, and that this interaction has a very important promoting effect on the CO oxidation reaction.

According to other studies in the literature, CuO could be located on titania and at the interface between the gold particles and the titania support or as patches on the gold particles. Based on EPR, XRD and XANES results, Liu et al. [29] proposed that particles under the CO oxidation reaction flow in reduced Au–Cu supported on SBA-15, prepared by a two-step adsorption method, were composed of gold particles decorated by a layer or patches of CuO, which maximized the perimeter between gold and CuO_x. CO adsorbed on gold would react with oxygen activated on neighboring CuO_x. In this way, the catalytic activity was greatly enhanced in comparison with monometallic gold. This is consistent with the fact that the plasmon band of Au–Cu/TiO_2 (Fig. 6Bc) evolved slightly differently from that of the Au/TiO_2 sample (Fig. 6Ba).

It has also been proposed [23,27] that CuO particles could reduce the size of gold particles, stabilize the Au particles, and facilitate the activation of molecular oxygen. The interaction between CuO and gold (Scheme 1c) enhances the catalytic activity as shown in Fig. 1. Moreover, the synergetic effect could result from the fact that Au/CuO is more active than Au/TiO_2. It has been proposed [23,27] that the CuO particles could facilitate the activation of molecular oxygen compared to TiO_2 and stabilize the gold particles. This is indeed what is observed during time on stream (Fig. 3).

As the Au:Cu ratio decreases, the CuO amount increases, so interaction of gold with CuO is favored, leading to an increasing activity. It may be noted that the particles of CuO are certainly very small since they could not be detected by XRD.

It must be noted that the catalytic activity, reaction rate and TOF, of our Au–Cu/TiO_2 catalysts measured at 30 °C and activated at 300 °C in air (Table 2) was very close to those of the Au–Cu/SiO_2 catalysts for similar reaction temperatures and particle sizes [26]. In contrast to the case of CO oxidation over monometallic gold catalysts, the use of a reducible support such as titania does not lead to Au–Cu catalysts much more active than those supported on non-reducible supports such as silica. This is a good indication that in the case of the Au–Cu/TiO_2 catalysts, the activation of oxygen preferably takes place on the copper oxide. This would rule out the hypothesis proposed by Carrettin et al. [76] that copper oxide species on the surface of TiO_2 would play a key role in stabilizing the defects of TiO_2, which could help to activate oxygen.

On the other hand, Fig. 1b shows that the temperature of activation under air had an important consequence on the catalytic activity since conversion increased as temperature increased and seems to be the highest after calcination activation at 300 °C in air. It is well-known that the catalytic activity of Au/TiO_2 catalysts in CO oxidation is very dependent on the gold particle size [77,78]. In calcined Au–Cu/TiO_2 catalysts, the average gold particle size increases with the activation temperature from 2.4 nm to 5.6 nm (Table 4). The decrease in activity after activation above 300 °C may be due to the increase in the gold particle size. Nevertheless, after activations at either 200 or 300 °C, the metal particle size does not drastically change; thus, the reason for the higher activity after calcination at 300 °C, observed previously in other systems such as Au–Cu supported on pure anatase or on pure rutile studied by our group (studies not yet published), may be due to a different chemical state of copper. As mentioned above (Section 4.1), copper is deposited on the support as copper hydroxide during deposition–precipitation, and it is known that copper hydroxide decomposes into CuO between 80 and 150 °C in air [79]. As mentioned above, after calcination at 200 °C, copper may therefore not be completely transformed into copper oxide yet.

Unlike calcined Au–Cu/TiO_2 catalysts, calcined Au–Cu/SBA-15 samples previously reported in [29] do not present catalytic activity at temperatures under 150 °C. This can be due to the different structure of the catalyst. For Au–Cu/SBA-15 samples, it is proposed that the metallic gold is in the core of the particle with a shell of CuO_x that blocks the active sites for CO oxidation, whereas in our

Au–Cu/TiO_2 catalysts, the Au sites are accessible for the reaction and in interaction with CuO that can activate molecular oxygen (Scheme 1c).

Whether the Au–Cu samples are treated in air or hydrogen, it is observed that the average metal particle sizes are not drastically different from those of Au/TiO_2 (Table 5). This differs from literature data, which shows that in Au–Cu catalysts, the particle size is smaller than in monometallic Au catalysts [23,29,30]. However, in those studies, the samples were prepared by methods different from the present one or were supported on other supports; moreover the reduction temperatures were higher than ours. For example, in Au–Cu/TiO_2 catalysts prepared by impregnation with 4 wt.% Au and Au:Cu = 1:3, after reduction in hydrogen a 400 °C, the metal particle size was much bigger (13 nm) than in our samples, and indeed smaller than in Au/TiO_2 (27 nm) [30]. In the case of Au–Cu/SBA15 catalysts reduced in hydrogen at 550 °C, the bimetallic nanoparticles had significantly reduced particle sizes (3.0–3.6 nm) compared with monometallic gold catalysts (5.7 nm) [26], but it is well known that gold poorly interacts with silica. In both cases, the size difference was explained by a sintering-resistant contribution of metallic Cu in the Au–Cu alloy nanoparticles.

The results of this study indicate than in Au–Cu catalysts, in addition to the metal particle size, the interaction between both metals, the homogeneity of the particles, the oxidation state of copper, the Au/Cu atomic ratio on the surface and, as consequence, the adsorption properties of the surface have an important influence on the catalytic activity of these catalysts in CO oxidation.

5. Conclusions

The new preparation method here proposed consisting in the successive deposition–precipitation with urea of copper then gold on titania is an efficient method to prepare Au–Cu catalysts because (i) it allows the deposition of gold preferentially on copper hydroxide, (ii) almost all gold and copper present in the solution on the support can be deposited, and (iii) the metallic particles are smaller than 3 nm: Au^0 is in interaction with CuO supported on titania after calcination and Au–Cu bimetallic particles are formed after reduction in hydrogen (Scheme 1). The latter system is less active in CO oxidation than monometallic Au/TiO_2, probably because of an inhibition due to the presence, or even an enrichment, of Cu atoms at the particle surface. In contrast, the calcined Au–Cu samples produce highly active and stable CO oxidation catalysts; they are 3 times more active than calcined Au/TiO_2 (according to the TOF measurements), probably because the gold particles directly interact with CuO, and CuO behaves as a better support for activating O_2 than TiO_2. It can be said that there is a promoting effect between Au^0 and CuO since the Au–Cu samples are more active than gold at temperatures at which Cu/TiO_2 is completely inactive (<75 °C).

Acknowledgements

The authors acknowledge financial support given by projects CONACYT 130407, Mexico, and PAPIIT 103513, UNAM, Mexico. We also thank Consejo Nacional de Ciencia y Tecnología, CONACYT and the ECOS-Nord program for funding the collaboration between Mexico and France (project #M10-P01). Alberto Sandoval gratefully acknowledges CONACYT for his PhD Scholarship. We also acknowledge Laurent Delannoy for technical support for some experiments performed in this study.

References

[1] J. Gong, Chemical Reviews 112 (2012) 2987–3054.
[2] C.L. Bracey, P.R. Ellis, G.J. Hutchings, Chemical Society Reviews 38 (2009) 2231–2243.
[3] R. Ferrando, J. Jellinek, R.L. Johnston, Chemical Reviews 108 (2008) 845.
[4] L. Guczi, G. Lu, Z. Zsoldos, Catalysis Today 17 (1993) 459.
[5] G.C. Bond, C. Louis, D.T. Thompson, Catalysis by Gold, vol. 6, 1st ed., Imperial College Press, London, 2006.
[6] M. Haruta, T. Kobayashi, H. Sano, N. Yamada, Chemistry Letters 2 (1987) 405–408.
[7] J. Gong, C.B. Mullins, Accounts of Chemical Research 42 (2009) 1063–1073.
[8] B. Roldan-Cuenya, Thin Solid Films 518 (2010) 3127–3150.
[9] P. Konova, A. Naydenov, C. Venkov, D. Mehandjiev, D. Andreeva, T. Tabakova, Journal of Molecular Catalysis A 213 (2004) 235–240.
[10] D. Andreeva, Gold Bull 35 (2002) 82.
[11] F. Yang, M.S. Chen, D.W. Goodman, Journal of Physical Chemistry C 113 (2009) 254.
[12] D.E. Starr, S.K. Shaikhutdinov, H.J. Freund, Topics in Catalysis 36 (2005) 33–41.
[13] M.C. Raphulu, J. McPherson, E. van-der-Lingen, J.A. Anderson, M.S. Scurrell, Gold Bull 43 (2010) 334–344.
[14] Y. Hao, M. Milhaylov, E. Ivanova, K. Hadjivanov, H. Knözinger, B.C. Gates, Journal of Catalysis 261 (2009) 137–149.
[15] Z. Zheng, J. Teo, X. Chen, H. Liu, Y. Yuan, R.R. Waclawik, Z. Zhong, H. Zhu, Chemistry – A European Journal 16 (2010) 1202–1211.
[16] C.K. Costello, J.H. Yang, H.Y. Law, Y. Wang, J.N. Lin, L.D. Marks, M.D. Kung, H.H. Kung, Applied Catalysis A 243 (2003) 15–24.
[17] H. Li, Y. Pei, X.C. Zeng, Journal of Chemical Physics 133 (2010) 134707.
[18] T.A. Baker, X. Liu, M. Friend, Physical Chemistry Chemical Physics 13 (2011) 34–46.
[19] J.D. Stiel, T.S. Kim, S.M. McClure, C.B. Mullins, Journal of the American Chemical Society 125 (2004) 2018.
[20] T.S. Kim, J.D. Stiehl, C.T. Reeves, R.J. Meyer, C.B. Mullins, Journal of the American Chemical Society 125 (2003) 2018.
[21] H. Liu, A.I. Kozlov, A.P. Kozlova, T. Shido, K. Asakura, Y. Iwasawa, Journal of Catalysis 185 (1999) 252–264.
[22] Z.-P. Liu, P. Hu, A. Alavi, Journal of the American Chemical Society 124 (2002) 14770–14779.
[23] X. Li, S.S.S. Fang, J. Teo, Y.L. Foo, A. Borgona, M. Lin, Z. Zhong, ACS Catalysis 2 (2012) 360–369.
[24] B. Zhu, Q. Gou, X. Huang, S. Wang, S. Zhang, S. Wu, W. Huang, Journal of Molecular Catalysis A 249 (2006) 211–217.
[25] X. Liu, A. Wang, X. Wang, C.Y. Mou, T. Zhang, Chemical Communications (2008) 3187–3189.
[26] X. Liu, A. Wang, T. Zhang, D.S. Su, C.Y. Mou, Catalysis Today 160 (2011) 103–108.
[27] J.C. Bauer, D. Mullins, M. Li, Z. Wu, E.A. Payzant, S.H. Overburry, S. Dai, Physical Chemistry Chemical Physics 13 (2011) 2571–2581.
[28] T.S. Mozer, D.A. Dziuba, C.T.P. Vieira, F.B. Passos, Journal of Power Sources 187 (2009) 209–215.
[29] X. Liu, A. Wang, L. Li, T. Zhang, C.Y. Mou, J.F. Lee, Journal of Catalysis 278 (2011) 288–296.
[30] R.J. Chimentao, F. Medina, J.L.G. Fierro, J. Llorca, J.E. Sueiras, Y. Cesteros, P. Salagre, Journal of Molecular Catalysis A 274 (2007) 159–168.
[31] N.K. Gamboa-Rosales, J.L. Ayastuy, M.P. González-Marcos, M.A. Gutiérrez-Ortiz, Catalysis Today 176 (2011) 63–71.
[32] N.K. Gamboa-Rosales, J.L. Ayastuy, M.P. González-Marcos, M.A. Gutiérrez-Ortiz, International Journal of Hydrogen Energy (2012), http://dx.doi.org/10.1016/j.ijhydene.2011.12.049.
[33] J. Lima-Fonseca, H.S. Ferreira, N. Bion, L. Pirault-Roy, M.D.C. Rangel, D. Duprez, F. Epron, (2012) 180, 34.
[34] P. Sangeetha, B. Zhao, Y.-W. Chen, Industrial and Engineering Chemistry Research 49 (2010) 2096–2102.
[35] S. Ajaikumar, J. Ahlksist, W. Larsson, A. Shchukarev, A.-R. Leino, K. Kordas, Applied Catalysis A 392 (2011) 11–18.
[36] L. Li, C. Wang, X. Ma, Z. Yang, X. Lu, Chinese Journal of Catalysis 33 (2012) 1778–1782.
[37] T. Pasini, M. Piccinini, M. Blosi, R. Bonelli, S. Albonetti, N. Dimitratos, G.J. Hutchings, F. Cavani, Green Chemistry 13 (2011) 2091–2099.
[38] L. Llorca, M. Domingez, C. Ledesma, R.J. Chimentao, F. Medina, J. Sueiras, I. Angurell, M. Seco, O. Rossell, Journal of Catalysis 258 (2008) 187–198.
[39] W. Li, A. Wang, X. Liu, T. Zhang, Applied Catalysis A 433/434 (2012) 146–151.
[40] R. Zanella, L. Delannoy, C. Louis, Applied Catalysis A 291 (2005) 62–72.
[41] R. Zanella, S. Giorgio, C.R. Henry, C. Louis, Journal of Physical Chemistry B 106 (2002) 7634–7642.
[42] R. Zanella, C. Louis, Catalysis Today 107/108 (2005) 768–777.
[43] A. Sandoval, A. Aguilar, C. Louis, A. Traverse, R. Zanella, Journal of Catalysis 281 (2011) 40–49.
[44] C.J.G. Van-Der-Grift, P.A. Elberse, A. Mulder, J.W. Geus, Applied Catalysis 59 (1990) 275–289.
[45] G.C. Bond, D.T. Thompson, Catalysis Reviews – Science and Engineering 41 (1999) 319–388.
[46] V. Idakiev, L. Ilieva, D. Andreeva, J.L. Blin, L. Gigot, B.L. Su, Applied Catalysis A 243 (2003) 25–39.
[47] A. Sandoval, A. Gómez-Cortés, R. Zanella, G. Díaz, J.M. Saniger, Journal of Molecular Catalysis A 278 (2007) 200–208.
[48] S. Velu, K. Susuki, M. Okasaki, M.P. Kapoor, T. Osaki, F. Ohashi, Journal of Catalysis 194 (2000) 373.
[49] F. Boccuzzi, A. Chiorino, G. Martra, M. Gargano, N. Ravasio, B. Carrozzini, Journal of Catalysis 165 (1997) 120–139.

[50] R. Zanella, S. Giorgio, C.H. Shin, C.R. Henry, C. Louis, Journal of Catalysis 222 (2004) 357–367.
[51] T. Del-Castillo-Castro, E. Larios-Rodríguez, Z. Molina-Arenas, M.M. Castillo-Ortega, J. Tanori, Composites, Part A 38 (2006) 107–113.
[52] J.A. Reyes-Esqueda, A. Bautista-Salvador, R. Zanella, J. Nanosci. Nanotechnol. 8 (2008) 3843–3850.
[53] O.G. Morales-Saavedra, R. Zanella, Materials Chemistry and Physics 124 (2010) 816–830.
[54] S. Tsubota, D.A.H. Cunningham, Y. Bando, M. Haruta, Studies in Surface Science and Catalysis 91 (1995) 227–235.
[55] X. Bokhimi, R. Zanella, A. Morales, V. Maturano, C. Ángeles-Chávez, Journal of Physical Chemistry C 115 (2011) 5856–5862.
[56] M. Mihaylov, H. Knözinger, K. Hadjiivanov, B.C. Gates, Industrial & Engineering Chemistry 79 (2007) 795.
[57] K. Chakarova, M. Mihaylov, S. Ivanova, M.A. Centeno, K. Hadjiivanov, Journal of Physical Chemistry C 115 (2011) 21273–21282.
[58] F. Boccuzzi, A. Chiorino, M. Manzoli, D. Andreeva, T. Tabakova, Journal of Catalysis 188 (1999) 176–185.
[59] F. Boccuzzi, A. Chiorino, M. Mazoli, Surface Science 454/456 (2000) 942–946.
[60] E. Roze, P. Gravejat, E. Quinet, J.L. Rousset, D. Bianchi, Journal of Physical Chemistry C 113 (2009) 1037–1045.
[61] G. Wu, N. Guan, L. Li, Catalysis Science & Technology 1 (2011) 601–608.
[62] A. Dandekar, M.A. Vannice, Journal of Catalysis 178 (1998) 621–639.
[63] O. Dulaurent, X. Courtois, V. Perrichon, D. Bianchi, Journal of Physical Chemistry B 104 (2000) 6001–6011.
[64] Y.-Y. Huang, Journal of the American Chemical Society 95 (1973) 6636–6640.
[65] K.I. Hadjiivanov, G.N. Vayssilov, Advances in Catalysis 47 (2002) 307–511.
[66] T.E. Shubina, C. Hartnig, M.T.M. Koper, Physical Chemistry Chemical Physics 6 (2004) 4215.
[67] T. Venkov, K. Hadjiivanov, Catalysis Communications 4 (2003) 209–213.
[68] G.A. Parks, Chemical Reviews 65 (1965) 177–197.
[69] J.W. Geus, A.J. van Dillen, in: G. Ertl, H. Knözinger, J. Weitkamp (Eds.), Handbook on Heterogeneous Catalysis, vol. 1, VCH, Weinheim, 1997.
[70] H. Okamoto, T.B. Massalski, Phase Diagrams of Binary Gold Alloys, ASM International, Metals Park, 1987.
[71] M. Hansen, Constitution of Binary Alloys, Mc Graw-Hill, New York, 1958.
[72] S.A. Maier, Plasmonics: Fundamentals and Applications, Springer Science + Business Media LLC, New York, 2007.
[73] K. Kreibig, M. Vollmer, Optical Properties of Metal Cluster, Springer, New York, USA, 1995.
[74] B.J. Auten, H. Lang, B.D. Chandler, Applied Catalysis B 81 (2008) 225–235.
[75] B.D. Chandler, C.G. Long, J.D. Gilbertson, C.J. Pursell, G. Vijayaraghavan, K.J. Stevenson, Journal of Physical Chemistry C 114 (2010) 11498–11508.
[76] S. Carrettin, Y. Hao, V. Aguilar-Guerrero, B.C. Gates, S. Trasobares, J.J. Calvino, A. Corma, Chemistry – A European Journal 13 (2007) 7771–7779.
[77] X. Bokhimi, R. Zanella, A. Morales, Journal of Physical Chemistry C 112 (2008) 12463–12467.
[78] M. Haruta, CATTECH 6 (2002) 102–115.
[79] J.Q. Qi, H.Y. Tian, L.T. Li, H.L.W. Chan, Nanoscale Research Letters 2 (2007) 107–111.